Physical processes controlling chlorophyll-a variability on the Mid-Atlantic Bight along northeast United States

Yi Xu[1], Travis Miles[2], and Oscar Schofield[2]

Corresponding author: Yi Xu (xuyi@sklec.ecnu.edu.cn)

[1] State Key Laboratory of Estuarine and Coastal Research, East China Normal University, 3663 Zhongshan Road North, Shanghai 200062, China.

[2] Center for Ocean Observing Leadership, Department of Marine and Coastal Sciences, School of Environmental and Biological Sciences, Rutgers University, 71 Dudley Road, New Brunswick, NJ, USA, 08901.

Abstract

We employed empirical orthogonal function (EOF) analysis to examine the spatial and temporal pattern changes in the surface chlorophyll a distribution (chl-a) on the Mid-Atlantic Bight (MAB) using Moderate Resolution Imaging Spectroradiometer Aqua (MODISA) chl-a data (2003-2016) and Sea-viewing Wide Field-of-view Sensor (SeaWiFS) chl-a data (1998-2007), and interpreted the underlying environmental determinants. A coupled physical-biogeochemical model was used to explore the primary physical factors determining the chl-a variability on the shelf. Model sensitivity studies identified wind mixing, net heat flux, and river discharge as the dominant factors influencing the MAB water column stability and consequent phytoplankton growth. The primary feature of chl-a indicated spring peaks on the outer shelf during the MODISA period, while fall-winter high during the SeaWiFS period in the same area. The observed increase in wind mixing and heat loss during winter and pre-spring were responsible for the delay in the phytoplankton bloom to spring on the outer shelf. The secondary chl-a peak occurred in the fall on the New Jersey shelf during MODISA period, and in the fall-winter in the Delaware Bay estuary for chl-a during SeaWiFS period. The Hudson River discharge was associated with the chl-a anomalies on the New Jersey shelf in the fall and winter during the MODISA period. Both the MODISA and SeaWiFS chl-a concentrations peaked during the fall-winter on the southern part of the MAB (in the EOF mode 3 region), but the MODISA chl-a peak area was north of the SeaWiFS chl-a peak area. The variation of chl-a concentration in the southern region of the MAB was most likely associated with the Chesapeake Bay rivers' discharge. In our study, the regional associations between chl-a and multiple climate-sensitive environmental parameters suggest that basin-scale forcing plays an important role in the underlying chl-a variabilities on the MAB.

Keywords

Ocean color; stratification/destratification; phytoplankton bloom; Mid-Atlantic Bight

1 Introduction

The Mid-Atlantic Bight (MAB) is a highly productive western boundary continental shelf. It is characterized by frequent phytoplankton blooms (Ryan et al., 1999; Yoder et al., 2001; Xu et al., 2011) that support diverse food-webs. Its high productivity supports one of the oldest fisheries in the United States (Powell & Mann, 2005), which continues to play a critical economic role for this region. For example, in 2015, the commercial fishery landings in New Jersey were worth $166 million, while those in the Mid-Atlantic region (New York through Virginia) were worth more than $500 million (NMFS, 2015). The fisheries of interest contain many migratory species. The timing of their migrations is tightly coupled to the shelf-wide thermal status, zooplankton and phytoplankton biomass, which are themselves tightly coupled to the annual thermal variability and associated hydrography on the shelf (Xu et al., 2013). Changes in the annual temperature structure

strongly influence the shelf's annual primary productivity (Schofield et al., 2008), zooplankton community composition (Bi et al., 2011; Friedland et al., 2013), and distribution of fish (Pinsky et al., 2013).

The MAB is a broad and gently sloping continental shelf. It extends from Cape Hatteras, NC in the south to Cape Cod, MA in the north. It is bounded offshore by a water mass known as the shelf-break front (Figure 1). On the shlef, the water is relatively shallow, with many of the nearshore regions being less than 60 m in depth. The shelf-break front is generally centered near the 200-m isobath (Wirick, 1994). Nearshore regions receive estuarine outflow from moderately sized, heavily urbanized rivers (the Hudson, Connecticut, Delaware, Susquehanna, Potomac, Choptank, and James rivers). These rivers are the major sources of fresh water, nutrients, and organic carbon for the MAB, and they control the physical and biogeochemical processes in this region (O'Reilly & Busch, 1984; Castelao et al., 2008a; Chant et al., 2008; Moline et al., 2008).

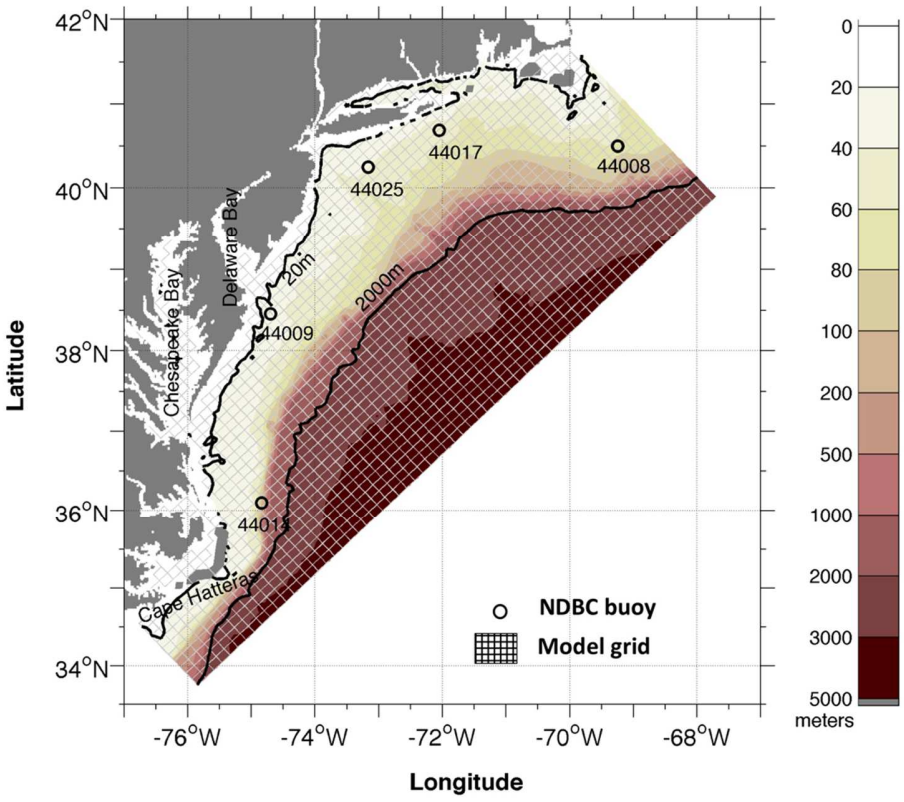

Figure 1. Bathymetry (color) and location map of the Mid-Atlantic Bight with overlapping numerical model grids. The black circles indicate the location of NDBC buoys. The black lines highlight the 20m and 2000m isobaths.

On seasonal and interannual time scales, the waters on the MAB exhibit considerable variability in temperature and salinity (Mountain, 2003; Castelao et al., 2010; Shearman & Lentz 2010). The MAB in the peak of summer has one of the largest vertical temperature gradients in the world, with water temperatures as high as 29 °C at the surface and as low as 8 °C on the shelf floor. This stratification forms in the late spring and early summer due to rapid seasonal surface warming and extends down to about 20 m across the entire shelf. The rapid warming isolates the remnant cold winter water as a continuous mid-shelf "cold pool" that extends from Nantucket to Cape Hatteras (Houghton et al., 1982; Biscaye et al., 1994). Associated with the water column stabilization, a spring phytoplankton bloom develops on the outer edge of the shelf and persists for several weeks before nutrients in the upper water column are depleted and zooplankton populations have increased (Xu et al., 2011). The cold pool persists throughout the summer and disappears during the fall overturn (Houghton et al., 1982). During the fall overturn, the water column is completely mixed in the shallow regions. This mixing returns nutrients to the surface waters and stimulates a fall phytoplankton bloom (Xu et al., 2013). The largest phytoplankton blooms on the MAB take place in the late fall and early winter (Ryan et al., 1999; Yoder et al., 2001; Xu et al., 2011). Time series of the coastal zone color scanner (CZCS) satellite data show that chl-a concentrations are highest during fall and winter in the continental shelf waters and that slope waters possess a secondary spring (Yoder et al., 2002). The magnitude of the fall-winter bloom is inversely related to the degree of storminess, which influences the degree of sustained water column mixing. The degree of mixing in turn determines the proportion of the phytoplankton that are severely light-limited (Xu et al., 2013). Thermal stratification re-develops as the frequency of winter storms decreases and the surface heat flux increases (Lentz et al., 2003), both of which induce phytoplankton blooms in the spring in the shallow surface mixed layer.

The interannual temperature and salinity of the water on the MAB appear to have undergone significant variation, with shelf waters becoming warmer and fresher in recent decades (Mountain, 2003; Shearman & Lentz, 2010). The changes along the northeast shelves have been observed from a variety of platforms (Shearman & Lentz 2010; Chen et al., 2014; Forsyth et al., 2015; Fulweiler et al., 2015). The temperature increases have been observed in both surface and bottom waters (Kavanaugh et al., 2017; Rheuban et al., 2017). The changes in temperature and corresponding water column stratification on the MAB are associated with the observed changes in phytoplankton biomass during the fall and winter (Schofield et al., 2008). These shifts are ecologically important, as the magnitude and timing of the blooms are critical for the rest of the ecosystem (Ryan et al., 1999; Yoder et al., 2002).

The changes in the weather and hydrography on the MAB have been hypothesized to result from several large-scale climate modes known to influence the northeast United States. The North Atlantic Oscillation (NAO), based on the differences between the strengths of

the Iceland low pressure system and the Azores high pressure system, is the mode dominating the winter climate variability over the upper North Atlantic Ocean on monthly to decadal scales (Hurrell, 1995; Hurrell & Deser, 2009). The positive phase of the NAO, during which there are increasing westerly winds, produces warmer temperatures on the MAB. It is associated with interannual variability in air-sea heat fluxes, depth of winter convection, and oceanic circulation (e.g., the displacement of the Gulf Stream meander) (Dickson et al., 1996; Curry & MaCartney, 2001; Marshall et al., 2001; Oschlies, 2001). The Atlantic Multi-decadal Oscillation (AMO) also has a major effect on the basin-scale dynamics in this region. The AMO is responsible for the frequency of severe Atlantic hurricanes (Trenberth et al., 2005), which play a role in the seasonal overturn of the MAB water column.

Many studies have focused on understanding the regional trends in atmospheric and oceanic patterns. Little attention has been given to how these regional environmental changes in combination with a changing climate system might influence regional primary production in the ocean. Remotely-sensed ocean color data are a valuable tool for examining the phytoplankton blooms on a regional scale (Platt et al., 2009). The CZCS and SeaWiFS chl-a data have been used to characterize the seasonal and spatial chl-a variability in this region. With the availability of decadal time series of ocean color data, it is now possible to study the temporal and spatial chl-a variability on longer scales. For this study, our goals are: (1) to identify the chl-a temporal and spatial patterns on the MAB using MODISA chl-a data from 2003-2016, and then compare with those obtained from SeaWiFS chl-a data from 1998-2006; (2) use a biophysical numerical model to identify the potential processes associated with stratification and destratification that might contribute to the observed chl-a variability; and (3) assess if the long-term trends in environmental parameters could explain the chl-a pattern changes in specific MAB regions. We will discuss the hydrographic and weather changes on the MAB and to what degree the chl-a variability can be explained by physical forcing under low-frequency climate cycles.

2 Materials and Methods

2.1 Ocean Color Remote Sensing Data

Chl-a distributions on the MAB were studied using Level-3 standard monthly-averaged composites of 9-km resolution SeaWiFS and MODISA data from January 1998 to December 2007 and from January 2003 to December 2016, respectively (https://oceancolor.gsfc.nasa.gov). The data are based on the ocean color reprocessing version 2014.0. The band ratio algorithms are based on the color index (OCI) of Hu et al. (2012). We chose monthly data to circumvent the omission of pixels due to clouds in the weekly chl-a imagery set, this allow us to maintain sufficient coverage to interpolate the seasonal and interannual variability. The overall spatial distributions of chl-a determined using the SeaWiFS and MODISA data were similar, with gradual decreases from the

coastal region to the shelf (Figures 2a, c). There were high standard deviations of chl-a in the coastal region, especially at the river mouths, suggesting that rivers are the dominant factor affecting the temporal chl-a variability in the nearshore regions (Figures 2b, d). The high standard deviations in the Nantucket Shoals were due to local winds, air-sea fluxes, tidal mixing, and shelf-wide circulation (Shearman &Lentz, 2004; Wilkin, 2006). Given the uncertainty in ocean color data to determine chl-a variability in Case-2 optically complex waters (i.e., increasing concentrations of color dissolved organic matter (CDOM) and total suspended matter (Bowers et al., 2011)), we excluded regions shallower than 20 m in the analysis. We also excluded water below 2000 m, as our focus in this study was on exploring the chl-a variability on the inner shelf and outer shelf (see Figure 1 for a map of the study area). Images with clouds covering more than 20% of the total area were excluded. In the valid images, pixels covered by clouds were replaced by the average of the eight surrounding non-cloud pixels. We performed this spatial averaging twice so that only pixels within 18 km of any missing pixel were used in the averaging process. We then filled in the remaining gaps using the corresponding monthly climatology data.

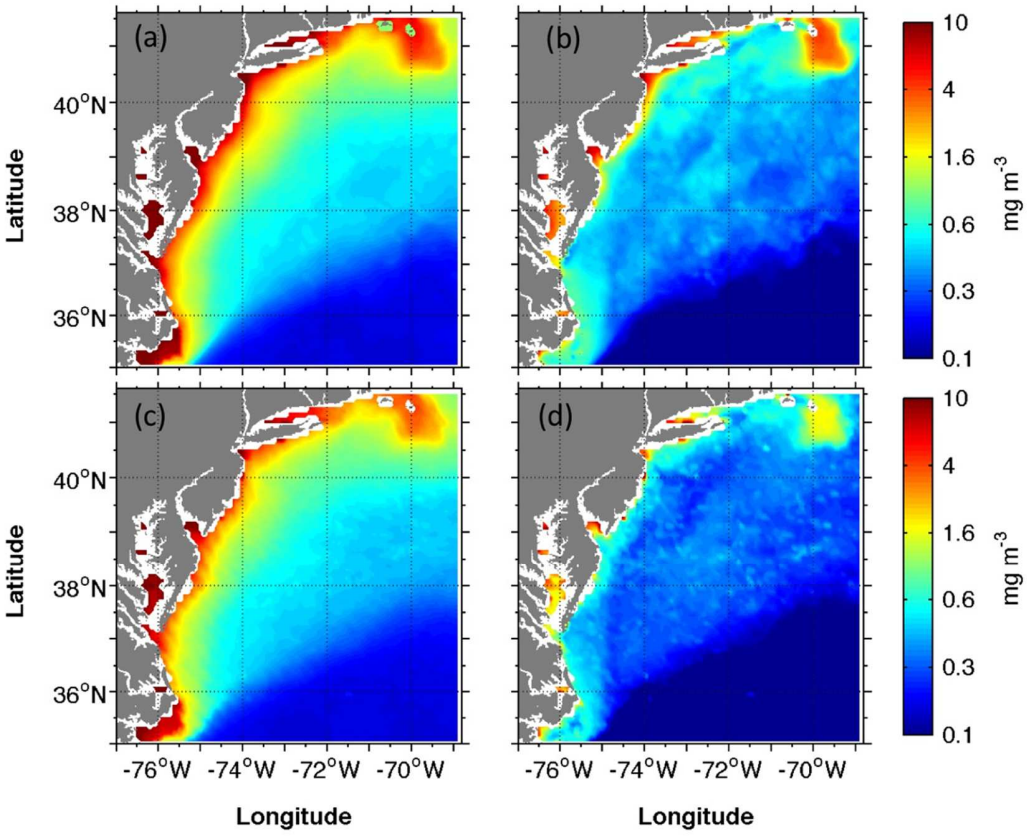

Figure 2. (a) Climatology of chl-a during the MODISA period (2003-2016). (b) Standard deviation of MODISA chl-a. (c) Climatology of chl-a. (d) Standard deviation of SeaWiFS chl-a.

To avoid directly compare the SeaWiFS and MODISA chl-a data based on different sensors, separate Empirical Orthogonal Function (EOF) analyses were performed for the SeaWiFS and MODISA chl-a time series to compress the spatial and temporal variability of each time series into a set of dominant modes with spatial functions and associated time-varying amplitudes. Different biogeographic zones on the shelf were obtained by the EOF analysis. Prior to the EOF analysis, the chl-a field was log-transformed and de-meaned by subtracting the whole time series mean of each pixel, for reducing the effects of areas with extreme high chl-a concentration and effects of strong seasonal signals in the time series.

2.2 Meteorology and River Data

In this study, we examined the relationship between the net heat flux anomaly and chl-a variability using the North American Regional Reanalysis (NARR) heat flux data produced by the National Centers for Environmental Prediction (NCEP) model, which assimilates a large amount of observational data to produce a long-term weather product over North America (Mesinger et al., 2006). The NARR monthly mean datasets with half-degree resolution were used in this study (https://www.ncdc.noaa.gov/nomads/data-products). The ocean net heat flux (NHF) consists of four components: shortwave radiation (SW); outgoing longwave radiation (LW); sensible heat flux from air-sea temperature differences (SH); and latent heat flux due to evaporation (LH). Thus, NHF = SW-LW-LH-SH.

To assess the variability in the local wind field, we used wind data from four moorings deployed by the National Data Buoy Center (NDBC) (http://www.ndbc.noaa.gov/maps/Northeast.shtml): moorings 44025 (40.25°N, 73.17°W); 44008 (40.50°N, 69.25°W); 44009 (38.46°N, 74.70°W); and 44014 (36.1°N, 74.84°W). Hourly data were averaged to give daily data. The daily river discharge data for 1998-2016 were downloaded from http://nwis.waterdata.usgs.gov/nwis. Seven major rivers were chosen: the Connecticut River; the Hudson River; the Delaware River; the Susquehanna River; the Potomac River; the Choptank River; and the James River.

2.3 Biogeochemical Model

We used a nitrogen-based biogeochemical model developed by Fennel et al. (2006), which has been integrated with the Regional Ocean Modeling System (ROMS) (Haidvogel & Beckmann, 1999; Wilkin et al., 2005; Wilkin & Hunter, 2013). Nitrogen was assumed to be the major limiting nutrient in the model based on nutrient budget studies that showed nitrogen limitation was frequently observed on the MAB (Ryther & Dunstan, 1971; Sharp & Church, 1981). The biogeochemical model was developed by Fennel et al. (2006). The basic structure followed the Fasham model (Fasham et al., 1990) and was constructed using seven state variables: phytoplankton; zooplankton; nitrate; ammonium; small and

large detritus; and phytoplankton chlorophyll. For more details, readers are referred to Fennel et al. (2006). The regional configuration used in this study covers the continental shelf of the MAB, with a horizontal grid resolution of approximately 5 km and 36 vertical layers in a terrain-following s-coordinate system (Figure 1). The model was driven by 3-hourly reanalysis atmospheric forcing data provided by the NCEP NARR. We used surface air temperature, pressure, relative humidity, 10-m winds, precipitation, downward longwave radiation, and net shortwave radiation to specify the surface fluxes of momentum and buoyancy based on bulk formulae (Fairall et al., 2003). At the open boundary, we specified temperature, salinity, nitrate (NO_3), total inorganic carbon (TIC), alkalinity, and oxygen using the climatology input data from the Fennel ROMS model simulation of the Northeast North American (NENA) shelf (Fennel et al., 2006; Hofmann et al., 2011). We included the inputs from the seven major rivers (listed in Section 2.2). The riverine inputs of temperature, salinity, and dissolved and particulate biological constituent concentrations were chosen based on the total nitrogen from Howarth et al. (1996). Representative riverine inputs were multiplied by the freshwater flow to give discharge rates, which were treated as time invariant for our simulations. The tidal harmonic variabilities (seven components: K1; O1; Q1; M2; S2; N2; and K2) were extracted from a regional advanced circulation model for oceanic, coastal, and estuarine water (ADCIRC) simulations.

The model was initialized from the output of another model in this study domain described in Hofmann et al. (2011). We conducted four-year simulations (2004-2007) that were spun up for one year and integrated for the subsequent 3 years (2005-2007). To test the sensitivity of the forcing on the water column stability and the corresponding influence on phytoplankton activity, four simulations (in addition to the control run, in which all forcing factors—rivers, wind stress, and net heat flux—were included) were carried out to investigate the individual effects of net heat flux, wind, and river discharge on the water column stability as well as on the timing and magnitude of the phytoplankton blooms. In each sensitivity run, we turned off the river, nutrients inputs from river, wind, and NHF on the day in the fall of 2005 when the NHF values switched from positive to negative to observe the contributions of the individual terms to the destratification/stratification as well as the blooms occurring during fall-spring of 2005-2006. We present the sensitivity experiment results from the fall-spring of 2005-2006 in this paper. The model validations are discussed in Xu et al. (2013).

3 Results

3.1 Biogeographic Zones

In the EOF analysis of the MODISA chl-a, three dominant modes of chl-a variability were identified. The first mode was responsible for 53% of the total variance was associated with the seasonality on the MAB. The mode possessed prominent peaks in the fall and

spring (March/April) (Figure 3g). The first EOF mode showed the seasonal changes in the offshore water deeper than 60 m in the outer shelf area (Figure 3a). The first EOF mode for the SeaWiFS chl-a was responsible for 51% of the total variance and had a spatial distribution similar to that of MODISA EOF mode 1 (Figure 3d). It differed from MODISA EOF mode 1 in that there was a fall-winter chl-a peak but no pronounced springtime peak (Figure 3j). By combining the EOF spatial coefficients and the percentages of the total variance for each EOF mode, we calculated the percentage of local variance explained by each mode. The results showed that the MODISA EOF mode 1 was responsible for up to 60% of the local variance in the outer shelf region (Figure 3a, circled area inside the red line), which is similar with the local region identified by SeaWiFS EOF mode 1 (Figure 3d, circled area inside the red line). The time series of the chl-a concentrations inside the circled area (spatial mean of all the pixels) showed the overall seasonal cycle of the spring chl-a peak for most of the years during the MODISA time period (2003-2016) (Figure 4a). This peak was anomalously high in 2011 and 2015. The spatial mean chl-a in the SeaWiFS period showed a fall-winter high in this region (Figure 4d).

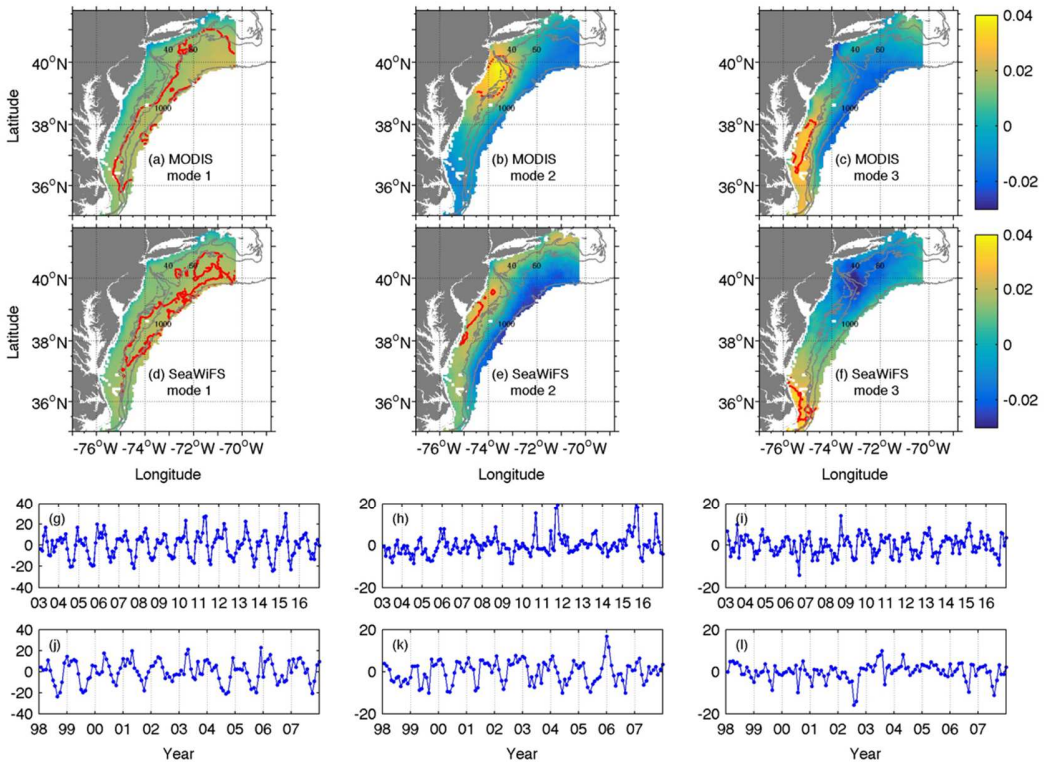

Figure 3. The first three EOF modes for the MODISA and SeaWiFS chl-a datasets. (a-c) Spatial coefficients of MODISA EOF modes 1-3. (d-f) spatial coefficients of SeaWiFS EOF modes 1-3. (g-i) temporal variabilities of MODISA EOF modes 1-3.

(j-l) temporal variabilities of SeaWiFS EOF modes 1-3. The red line on each contour map indicates the significant biogeographic zone associated with each mode.

The second EOF MODISA chl-a mode was responsible for 10% of the total variance. The spatial coefficient was positive on the New Jersey shelf and negative offshore (Figure 3b). There was a pronounced positive temporal amplitude in fall for the second EOF mode (Figure 3h). Thus, combined with the positive spatial coefficient, there was an increase in the amount of chl-a on the shelf in the fall. The second EOF SeaWiFS chl-a mode was responsible for 13% of the total variance. The 60-m isobath divided the MAB into two regions, with the spatial coefficient positive on the inner shelf and negative on the outer shelf. This indicated that the chl-a concentrations were high on the inner shelf from Cape Hatteras, NC to Cape Cod, MA (Figure 3e) during the fall and winter. The second MODISA mode, with pronounced fall peaks, was responsible for 30% of the local variance on the New Jersey shelf region (Figure 3b, circled area inside the red line; Figure 4b). The second SeaWiFS EOF mode was responsible for 30% of the local variance in the Delaware Bay estuary (Figures 3e, red line), and was associated with high chl-a concentrations during the fall and winter (Figure 4e).

The third MODISA and SeaWiFS modes were responsible for 9% and 8% of the total variance, respectively, representing a zone of positive spatial variance in the southern part of the MAB. On the coastal waters near Virginia and further south near Cape Hatteras, the third MODISA and SeaWiFS modes were responsible for a high local variance (up to 30%) (Figure 3c, red line and Figure 3f, red line). The spatial mean chl-a indicated the seasonal fall-spring high (Figure 4c, f), possibly associated with coastal river inputs at these areas.

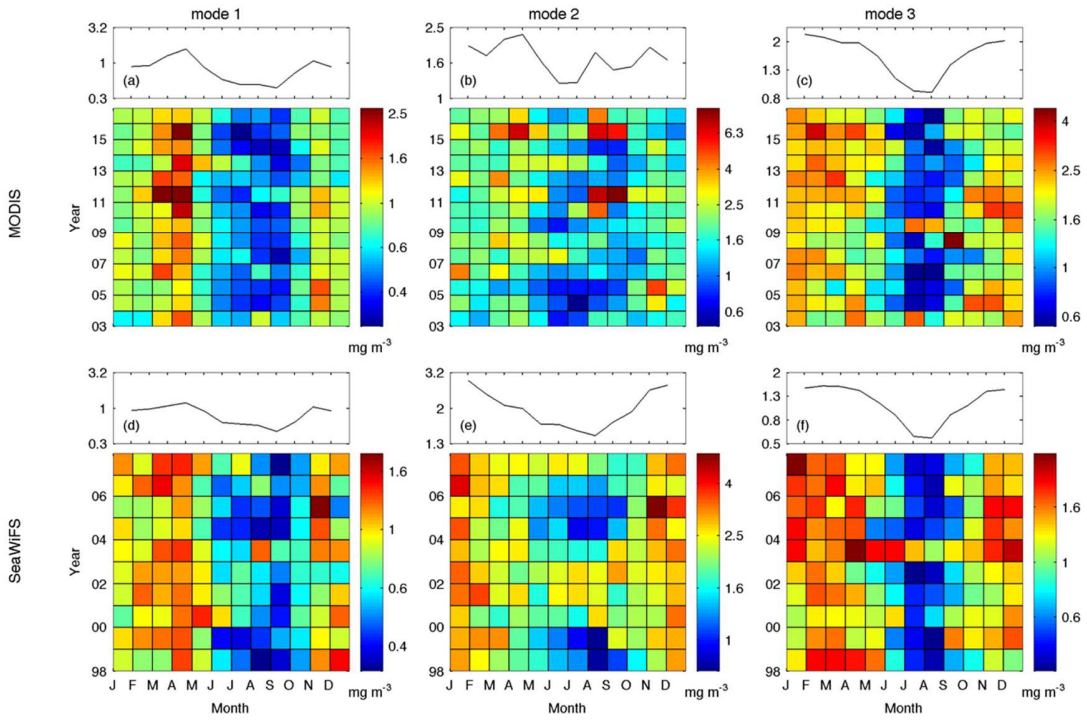

Figure 4. Comparison of the monthly mean chl-a concentrations in the biogeographic zones defined by MODISA and SeaWiFS EOF modes 1-3. The climatological seasonal cycles of the chl-a concentrations in the biogeographic zones are plotted on top of each panel.

One could determine the overall chl-a distributions on the MAB from the first three EOF modes. The biogeographic zones of the EOF mode 1 were on the outer shelf for both datasets. However, the seasonal signals varied: there was a large spring chl-a peak during the MODISA period and fall-winter high chl-a during the SeaWiFS period. The biogeographic zones corresponding to the second EOF mode presented at different locations: large portions of the local variance presented in the New Jersey shelf in the second MODISA EOF mode, and the Delaware Bay estuary explained much of the local variance with fall-winter high chl-a in the SeaWiFS EOF mode 2 region. The two biogeographic zones identified by the third EOF modes were different, however, the temporal signals corresponding to the fall-winter chl-a high were similar for the two zones. EOF analysis applied to the MODISA and SeaWiFS chl-a data individually yielded different biogeographic zones on the MAB. The zones on the outer shelf were in similar locations but had different seasonal signals, while on the inner shelf, most of the biogeographic zones from the two datasets were in different locations, suggesting that the physical regulation of biological responses was not temporally or spatially coherent on the MAB from 1998 to 2016. Next, we assessed how environmental changes in the MAB were

responsible for the spatial and temporal patterns of phytoplankton growth over the last 20 years.

3.2 Terms Influencing Water Column Stability and Phytoplankton Bloom

To determine the dominant factors driving phytoplankton bloom dynamics, we conducted a series of numerical sensitivity studies to test the relationship between stratification/destratification and the phytoplankton bloom. Phytoplankton dynamics on the MAB are driven by the overall stratification of the water column (Xu et al., 2013). The most important factors that determine the water column stability in the MAB are solar heating, freshwater input-related density stratification, and mixing by wind. Assuming that the stratifying effects of heating and buoyancy inputs and the mixing produced through cooling, wind, and tides act independently, the joint effect of these processes will determine the overall water column destratification/stratification. In order to assess the balance between the processes that mix the water column and those that stabilize it, we calculated the potential energy anomaly (PEA) of the water column and used its diagnostic terms to investigate the water column stability. Simpson et al. (1977) (see also Simpson & Bowers, 1981) defined the PEA as follows:

$$\phi = \int_{-h}^{\eta} gz(\bar{\rho} - \rho)\, dz/D \quad (1)$$

where $D = \eta + h$ denotes the depth of the water column. $\bar{\rho}$ denotes the depth-mean density, ρ represents the density, and $\bar{\rho} = \int_{-h}^{\eta} \rho\, dz/D$.

The PEA is zero for a fully mixed water column, positive for stable stratification, and negative for unstable stratification. Physically, the PEA gives the amount of energy per volume that is necessary to vertically homogenize the entire water column. To determine whether the water column remains stratified or mixes as a result of the forces acting on it, we calculated the change of PEA with time (Simpson & Bowers, 1981):

$$d\phi/dt = \alpha g Q/2c + g(E - P)\Delta\rho/2 - \varepsilon\kappa_b\rho\overline{|u_b|^3} - \delta\kappa_s\rho_s\,\overline{W^3}/h + (g\partial\rho/\partial y)\int_{-h}^{0}(v - \hat{v})\, zdz/h \quad (2)$$

The first two terms on the right hand side represent the change in water column stability due to net surface solar heat at a rate Q, salt flux due to evaporation (E), and precipitation (P), while the third and fourth terms represent the stirring due to tidal currents (u_b) and wind speed (W). Here, α and c are the thermal expansion coefficient and specific heat of seawater, respectively, and ρ_s is the air density. ε and δ denote the corresponding mixing efficiencies, and κ_s and κ_b are the effective drag coefficients for the surface and bottom stresses, respectively. The last term represents the influence of freshwater inputs from rivers on water column stability. For horizontal flows across the shelf (in the cross-shelf direction), the density gradient across the shelf drives a shear flow circulation with low-density water flowing offshore at the surface. The contribution of such a shear flow to the PEA is represented by the last term, which allows us to

calculate an input of ϕ for any known velocity field in the cross-shelf direction (v is the velocity at the cross-shelf direction, $\hat{v}$ is the depth averaged velocity). The order of magnitude of each term represents the importance of the input to ϕ. The net heat flux, wind mixing, and river runoff terms have the same orders of magnitude (10^{-5}), while the tidal mixing (10^{-7}) and salt flux (10^{-6}) terms are much smaller. Thus, the net heat flux, wind mixing, and river runoff terms are the processes that are primarily responsible for stratification/destratification on the MAB.

Phytoplankton blooms are sensitive to water column stability, changes in nutrient supply, and light availability. We conducted several sensitivity studies to assess the influence of water column stability on the timing and magnitude of phytoplankton blooms in the model. Some processes, such as river runoff, not only affect buoyancy by providing low-salinity water but also produce nutrient-rich water on the continental shelf (Moline et al., 2008). Therefore, we conducted two sensitivity experiments to study the influences of rivers on phytoplankton growth. In Experiment 1, no river inputs were included in the simulation. In Experiment 2, we kept the river inputs as temperature and salinity mass sources/sinks term, but turn off the input of nutrients from river. The influence of the NHF on the phytoplankton blooms was tested in Experiment 3 by removing the net heat flux on the day in fall when the NHF turned from positive to negative. The experiment indicated that there was no mixing due to heat loss, thus, destratification of the water column occurred through wind mixing. To assess the importance of wind mixing in phytoplankton blooms, the wind forcing was turned off in Experiment 4. These experimental results were compared with the "control" run results, in which all the forcing factors were included. Figure 5 shows the results for fall-spring 2005-2006.

The model successfully simulated the destratification in the fall, which was accompanied by the initiation of a fall bloom on both the inner shelf (identified by EOF mode 2, Figure 3) and outer shelf (identified by EOF mode 1, Figure 3) regions in the control run using the forcing functions (Figure 5a, black line). On the inner shelf, the bloom lasted throughout the winter, during which the water column was well-mixed (PEA was low). The bloom dissipated in the spring soon after the water column stratified. On the outer shelf, chl-a concentrations decreased over the winter but increased in the spring with the increase of PEA (Figure 5c, black line), presumably due to limited light availability in the deeply mixed water column in the winter and increased light availability in the spring when the water column stratified.

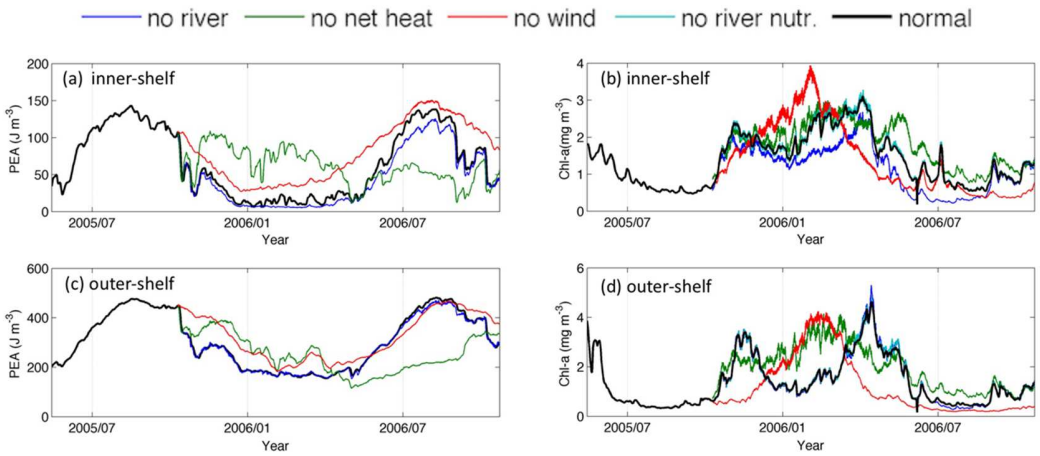

Figure 5. Model sensitivity study of the factors influencing the water column stability and the timing and magnitude of the blooms. The potential energy anomaly (PEA) represents the water column stability. (a, b) inner shelf PEA and changes in the chl-a concentrations under different forcing. (c, d) outer shelf PEA and chl-a concentration changes under different forcing.

Model simulations showed that the timing of the destratification and initiation of the fall bloom were closely related to the wind forcing on both the inner and outer shelf. When the wind forcing was turned off in the simulation (Figure 5, red line), the timing of the stratification process and initiation of the fall bloom was delayed. This agrees with previous observations of chl-a activity on the MAB that the timing of destratification on the shelf are more associated with wind mixing (Lentz et al., 2003; Castelao et al., 2008b). During the winter months, there was a significant increase in the blooms' magnitudes in the scenarios in which there was no wind or no net heat flux. Due to weaker mixing and corresponding increase in light availability, the "no wind" or "no cooling" conditions could allow for larger winter blooms. The concentrations of chl-a did not change when the nutrient inputs from the rivers were turned off (Figure 5, light blue line). While the river nutrients did not appear to play a major role in increasing phytoplankton productivity, the river's role in increasing water stability on the inner shelf was significant, as evidenced by the decline in chl-a concentrations when the inputs of low-salinity riverine water were removed (Figure 5b, blue line). The river inputs did significantly affect the magnitudes of the winter blooms, especially in the inner shelf region (Figure 5b, blue line). Without wind, the stratification occurred earlier in the spring, especially on the inner shelf. Under this condition, there was no spring bloom in either the offshore or near-shore regions, due to the winter bloom had already used up all the nutrients. When the net heat flux was removed, the water was neither cooled in the winter nor heated in the spring. The PEA of the water on both the inner and outer shelves

increased in winter (Figure 5a, c, green lines). The “no cooling” condition stabilized the water column, which stimulated the growth of phytoplankton during the winter on the MAB (Figure 5b, d, green lines). Because heating aids in the stratification of the water column, “no heating” in the spring decreased the water column’s PEA. The outer shelf springtime phytoplankton bloom was most affected by this phenomenon. There was no obvious spring bloom due to delayed springtime stratification on the outer shelf (Figure 5d, green line). Therefore, the model sensitivity study suggests that the influences of the net heat flux on the PEA and blooms are significant on the outer shelf, that the increased buoyancy due to river inputs is significant on the inner shelf, and that wind mixing plays an important role in both the timing and magnitude of the fall and spring blooms.

To interpret the relationship between water column stability and biological productivity, it is crucial to understand both the long-term changes in the physical drivers and the spatial and temporal structures of any correlations that do exist between the physical forcing and the biological signals. The interannual changes in the effects of major physical forcing on stratification and the associated chl-a variability were examined.

3.2.1 Net Heat Flux

The impacts of surface heating and cooling on phytoplankton productivity were assessed by examining the relationships among the chl-a concentrations and NHF anomalies during the time periods over which the MODISA and SeaWiFS chl-a studies were performed. Because the correlations among chl-a and the NHF changed from positive to negative during the annual stratification-destratification cycle, the pixel-by-pixel correlations among the NHF and chl-a anomalies for the whole time series were relatively low (Figures 6a, b). Significant positive correlations were found over much of the outer shelf of the MAB during both the MODISA and SeaWiFS periods (Figures 6a, b, black contour), where the dominant biogeographic zones were identified by EOF mode 1 (Figures 3a, d). Time series of the spatial mean NHF and chl-a anomalies in this region during the winter and pre-spring months showed significant positive correlations (Figures 6c, d: $r = 0.69$, $p < 0.01$; $r = 0.79$, $p < 0.01$ for the MODISA and SeaWiFS periods, respectively). This implies that the influence of the NHF on chl-a variability on the outer shelf region is highly significant in winter to pre-spring. This is consistent with the results in our model sensitivity studies of the influence of the NHF on chl-a variability, in which the reduced winter/pre-spring water column stability inhibited phytoplankton growth. Conversely, a high NHF during the winter to pre-spring period stimulated an increase in the amount of chl-a in the water column.

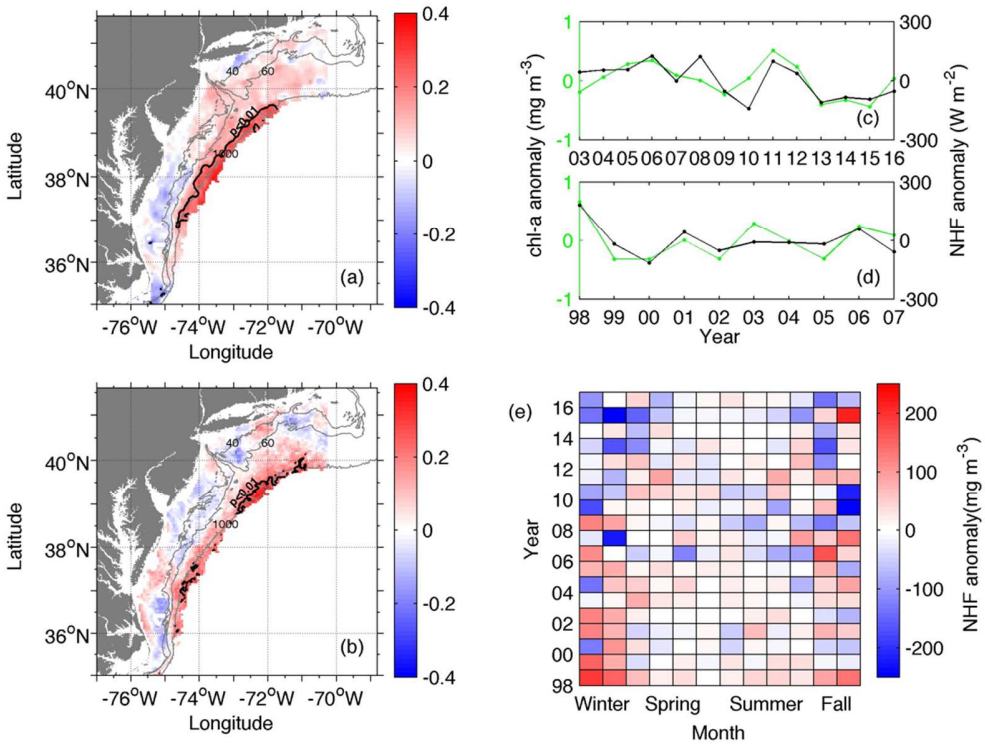

Figure 6. Comparison of chl-a and NHF anomalies. (a) correlation coefficients of chl-a and NHF anomalies during the MODISA period. The black lines specify the significant correlated area with $r > 0.3$ and $p < 0.01$. (b) for the SeaWiFS period. (c) time series of the winter to pre-spring spatial mean chl-a (green line) and NHF (black line) anomalies in the significant correlated area for the MODISA period. (d) for the SeaWiFS period. (e) NHF anomaly in different seasons during 1998-2016.

Throughout the NHF interannual time period of 1998-2016 (Figure 6e), high frequency of anomalously low NHF values were observed in the last ten years (mostly during fall to pre-spring (October to February)). Our EOF analysis of the spatial and temporal chl-a variability in this region showed that the fall-winter chl-a peak during the SeaWiFS period was replaced by chl-a peaks in the spring during the MODISA period. This change could be due to the NHF anomalies mentioned above, which are associated with more cooling. A negative NHF during the winter to pre-spring period is associated with increased heat loss and enhanced winter convection mixing, which delay the onset of stratification and result in a delayed chl-a peak in the spring. During the SeaWiFS period, relatively high NHF in the winter decrease the turbulent convection, stabilizing the upper mixed layer and stimulating phytoplankton growth during the light-limited winter (Xu et al., 2011). By studying the connections among the chl-a and NHF anomalies, we conclude that the

relatively high NHF anomalies that are associated with decreased heat loss likely promote blooms in the winter, as observed during the SeaWiFS period. The relatively low NHF anomalies (associated with more heat loss) observed in the winter and pre-spring during the MODISA period inhibit winter blooms, delaying them until spring when there is enough stratification to keep the phytoplankton in the euphotic zone.

3.2.2 Wind

The wind data collected from five NDBC buoys (44008, 44009, 44014, 44017, and 44025) from 1998 to 2016 were used to assess the overall wind mixing on the MAB. We calculated the monthly mean wind speed along with the storm frequency (percentage of days in a month during which the wind speed was higher than 10 m s^{-1}) using the average of the data from the five buoys. The seasons were defined as follows: winter (December-February); spring (March-May); summer (June-August); and fall (September-November). Overall, the long-term variabilities of wind speed and storm frequency were significant (Figure 7). In the fall, the average wind speed and storm frequency reveal a linear interannual increasing trend increased over the time period. In the winter, the wind speed was higher than it was in the other seasons, which was due to an increase in the frequency of storms over time (Figure 7b). The increasing trend in wind speed and storm frequency were significant in the winter season as well. The wind speed was consistently lower during the spring and summer, and no trended interannual variability were found over the time period of 1998-2016 (Figures 7c, d).

The wind direction also plays an important role in the seasonal wind-driven circulation on the shelf (Gong et al., 2010). We assessed the long-term variabilities in the wind directions on the MAB by observing the changes in the dominant wind directions along the time series (Figures 8 a-d). We used the 44025 buoy data for the analysis because of its location and temporal coverage. For the seasonal variabilities, we observed seasonal switch from a prevailing northwesterly (NW) wind during fall-winter (Figures 8a, b, orange line) to a persistent southwesterly (SW) wind in spring-summer (Figures 8c, d, blue line). The frequency of the NW winds ranged from 35-68% in the winter. The NW winds drive cross-shelf flow, provide favorable conditions for the transport of fresh coastal water offshore, and contribute to stratification on the inner shelf (Gong et al., 2010). The summer period was dominated by upwelling-favorable SW winds, and no significant trends were observed over time. The directions of the wind were relatively evenly distributed during the fall and spring for each year. In the fall, the NE winds occurred with increasing frequency along the time series ($y=0.01x-20.05$, $p=0.01$). The along-shelf NE winds generate strong down-shelf flows and could be a possible driver for the bloom observed on the New Jersey shelf during the recent MODISA period.

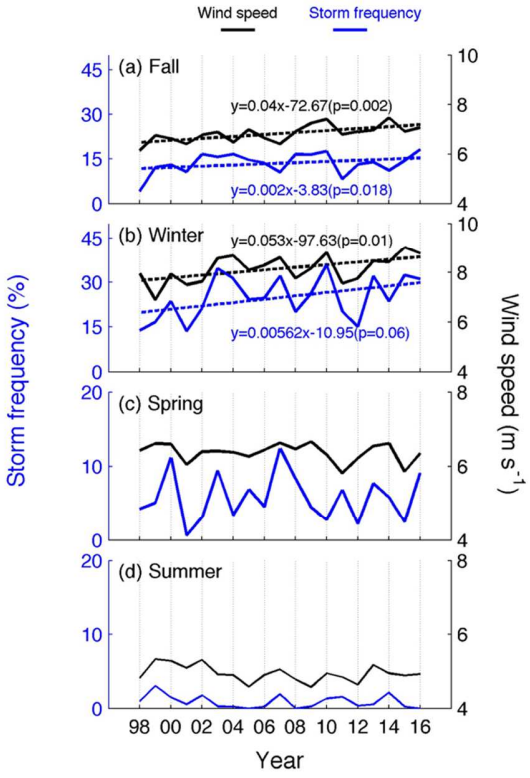

Figure 7. Time series of wind speed (black dashed line) and storm frequency (blue dashed line), with their trend lines (solid).

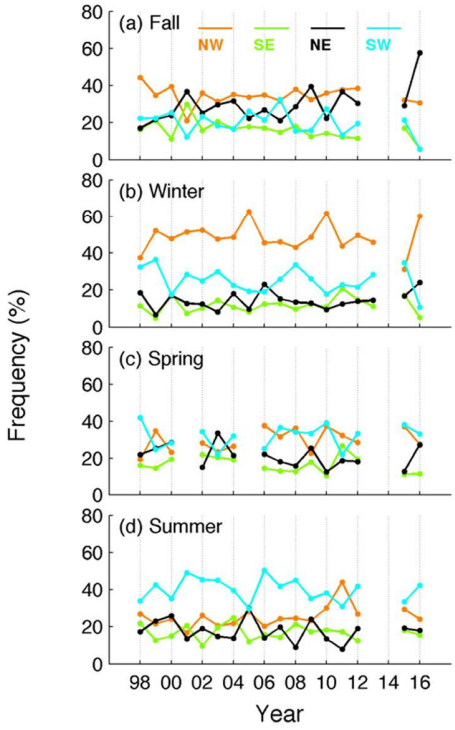

Figure 8. Time series of the frequency of the different wind directions for each season.

3.2.3 River

Rivers integrate environmental change factors, both natural and anthropogenic. Regional climate change can influence seasonality, size, and the outflow of rivers. The biogeographic zones identified by EOF modes 2 and 3 were on the inner shelf and close to major river estuaries on the MAB. In order to check the influence of river outflows on chl-a variability, the seasonal climatology of the major rivers' discharges into the MAB region were examined. We recall that the rivers studied were the Connecticut River, Hudson River, Delaware River, and Chesapeake Bay rivers (the discharges from the Susquehanna River, Potomac River, Choptank River, and James River were averaged to obtain the outflow from the Chesapeake Bay). To evaluate the influence of the rivers' inputs on the chl-a pattern changes on seasonal and interannual scales, we first compared the monthly climatology of the river discharge during the MODISA and SeaWiFS periods (Figure 9). In both periods, the averaged maximum discharge was in spring (April). It decreased in the summer and increased again in the fall. In comparing the monthly climatology of the two time periods, it was found that there were higher discharges from September to December during the MODISA period, particularly from the Hudson River and Chesapeake Bay rivers (Figure 9a, d, red line). The wind-driven circulation along with the Hudson River runoff has been shown to influence the stratification on the inner shelf off of New York/New Jersey (Chant et al., 2008). Thus, high discharge events in the fall and winter

were associated with nutrient input and the onset of stratification in the upper layer, which could explain the magnitude of the phytoplankton blooms on the New Jersey Shelf during the MODISA period. The Chesapeake Bay outflow turns to the south along the Virginia coast and acts as the major influence on the biogeochemistry in that area through its effect on stratification and nutrient loading (Friederichs et al., 2019). Therefore, the chl-a variabilities identified by EOF mode 3 could be related to the variabilities in the rivers' discharges from the Chesapeake B

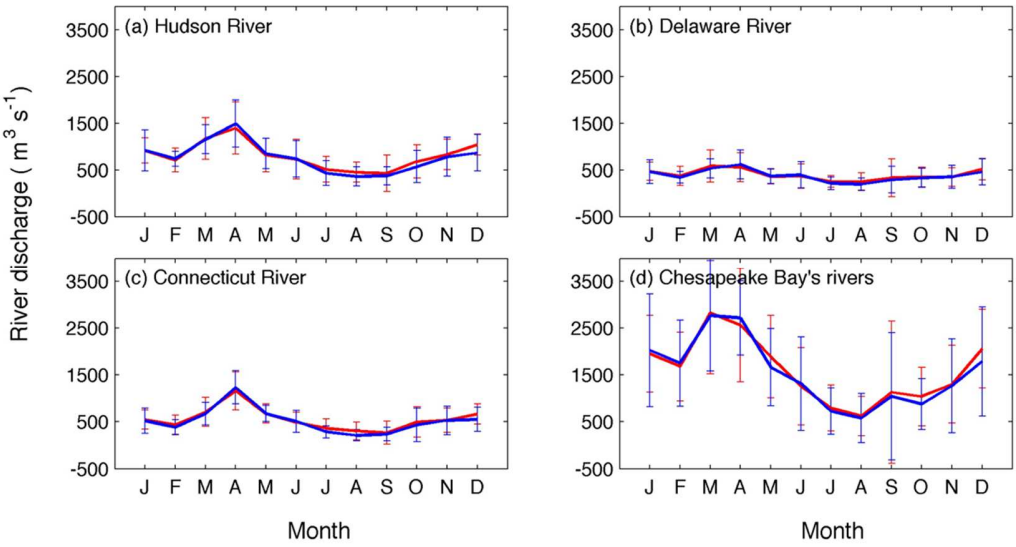

Figure 9. Climatology and standard deviation of monthly river discharge. The red line indicates the MODISA period, and the blue line indicates the SeaWiFS period.

To determine the influence of river plumes on interannual chl-a variability during the MODISA and SeaWiFS periods, the time series of the rivers' discharge anomalies were compared with the chl-a anomalies in the near shore region, which was in the regions identified by EOF modes 2 and 3 (Figure 10). To assess the influence of the Hudson River, the MODISA chl-a anomalies in the EOF mode 2 region (Figure 3b, New Jersey shelf, enclosed by red line) were compared with the Hudson River discharge time series (Figure 10a), and a statistically significant positive correlation was found between the two time series ($r = 0.26$, $p < 0.001$). By comparing Chesapeake Bay rivers' discharge with the chl-a anomalies in the MODISA EOF mode 3 region (Figure 3c, Virginia coast, enclosed by red line), it was found that the chl-a anomalies were positively correlated with the Chesapeake Bay rivers' discharge (Figure 10b; $r = 0.34$, $p < 0.001$). There was also a high positive correlation between the Chesapeake Bay rivers' discharge and the chl-a time series in the SeaWiFS EOF mode 3 region (Figure 10d; $r = 0.60$, $p < 0.001$). The strong correlation between the two time series is most likely due to the fact that at the Chesapeake Bay outflow plume area (SeaWiFS EOF mode 3) (Figure 3f, Cape Hatteras coast), a high-nutrient offshore plume expansion promotes phytoplankton accumulation (Jiang &

Xia, 2018; Friederichs et al., 2019). Throughout the time series, less significant correlations were found between the Delaware River discharge and chl-a anomalies in the SeaWiFS EOF mode 2 region.

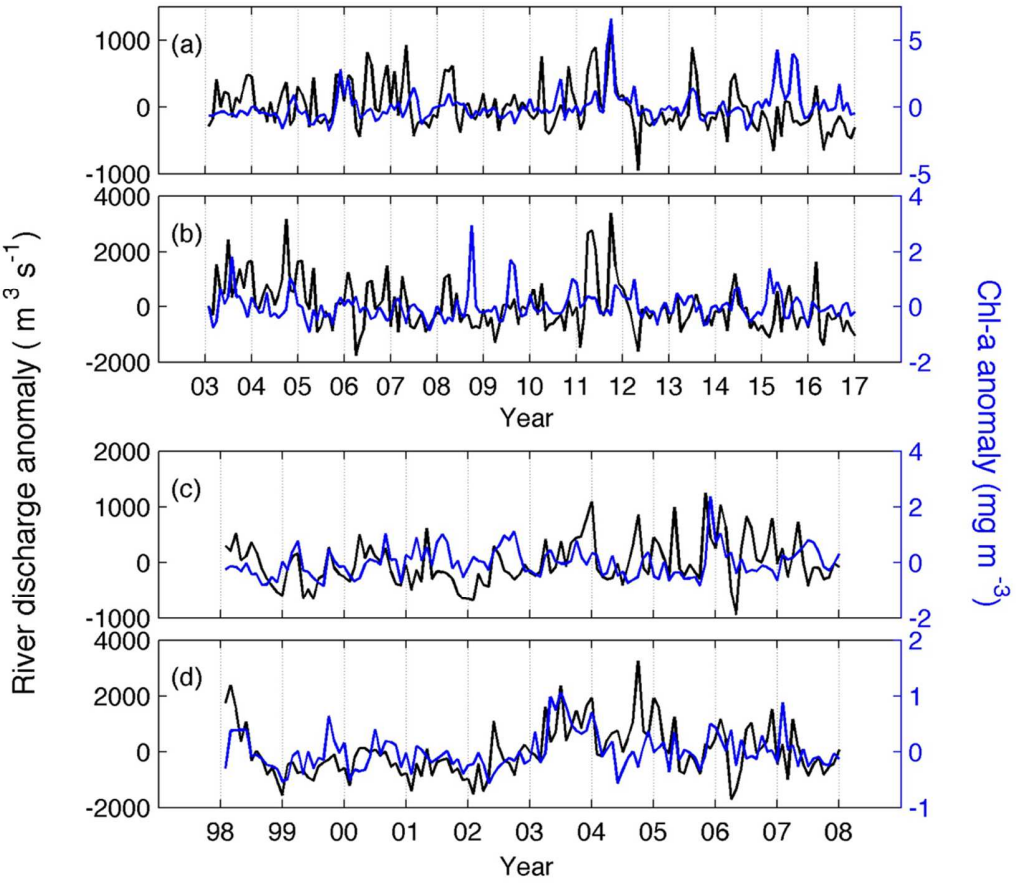

Figure 10. Time series of river discharge anomalies (black) and chl-a anomalies (blue): (a) comparison of the Hudson River with the chl-a anomaly for the zone in Figure 3b. (b) comparison of the Chesapeake Bay rivers with the chl-a anomaly for the zone in Figure 3c. (c) comparison of the Delaware River with the chl-a anomaly for the zone in Figure 3e. (d) comparison of the Chesapeake Bay rivers with the chl-a anomaly for the zone in Figure 3f.

In addition, month by month correlations between river discharges and chl-a anomalies were calculated using the same date sets (Table 1). During the MODIS period, there were significant correlations between the Hudson river discharge and the chl-a anomalies on the New Jersey shelf in September (r = 0.73) and January (r = 0.53) and in October (r = 0.67) and December (r = 0.52) that indicated a connection between the Chesapeake Bay outflow and the Virginia coast chl-a anomalies. High correlations were also noted between the Chesapeake Bay outflow and the chl-a time series along the coast off of Cape Hatteras in most of the fall and winter months during the SeaWiFS period. These results are consistent

575 with our interpretation of the way in which riverine-influenced stratification stimulates
576 the phytoplankton bloom over the fall-winter on the inner shelf.

577 **Table 1.** The correlation coefficients of the monthly river discharge anomalies and chl-a
578 anomalies in the biogeographic zones identified by EOF mode 2 and mode 3. p values are
579 shown in the parenthesis. The bold values indicate the significant correlation.

Variables	Correlation coefficient			
	MODISA period (2003-2016)		SeaWiFS period (1998-2007)	
Month	Chl-a (mode 2)- Hudson River	Chl-a (mode 3)-Chespeckbay	Chl-a (mode 2) - Delaware River and Connetitute River	Chl-a (mode 3)-Chespeckbay
Jan.	**0.53 (0.04)**	0.30 (0.29)	0.42 (0.22)	0.36 (0.31)
Feb.	0.24 (0.41)	-0.41 (0.14)	0.21 (0.57)	**0.65 (0.04)**
Mar.	-0.18 (0.53)	-0.32 (0.26)	-0.02 (0.95)	0.09 (0.80)
Apr.	0.06 (0.85)	0.39 (0.17)	0.36 (0.30)	**0.63 (0.05)**
May	0.16 (0.59)	0.31 (0.28)	0.54 (0.10)	0.07 (0.85)
Jun.	0.18 (0.53)	0.30 (0.3)	-0.10 (0.79)	**0.77 (0.008)**
Jul.	0.28 (0.32)	0.02 (0.94)	-0.22 (0.54)	0.31 (0.39)
Aug.	0.29 (0.32)	0.25 (0.40)	0.09 (0.81)	**0.65 (0.04)**
Sep.	**0.73 (0.003)**	-0.06 (0.83)	0.11 (0.75)	0.10 (0.79)
Oct.	0.23 (0.43)	**0.67 (0.008)**	0.11 (0.75)	**0.66 (0.04)**
Nov.	0.20 (0.49)	0.06 (0.83)	0.43 (0.22)	**0.65 (0.04)**
Dec.	0.28 (0.33)	**0.52(0.08)**	0.26 (0.46)	**0.71 (0.02)**

580
581

4 Discussion

4.1 Water Column Stability and Chl-a in MAB

Estimating the long-term trends of chl-a variabilities based on combined chl-a datasets from different satellite sensors is difficult, because the uncertainties of the derived chl-a products from the different sensors (Gregg et al., 2010; Hammond et al., 2018). Therefore, we applied EOF analysis to the MODISA and SeaWiFS chl-a datasets separately to reduce the chl-a data set to the dominant modes, and examine their associated spatial and temporal pattern changes. To explore the underlying factors contributing to such pattern changes, we compared the variances of the physical forcing mechanisms responsible for the chl-a variabilities over time. The spatial modes, which were consistent throughout both the MODISA and SeaWiFS periods, divided the study area into the outer shelf and the inner shelf. Combining the spatial pattern information with the amplitudes of the time series, we showed that on the outer shelf, there were seasonal spring peaks in the MODISA chl-a, while there were fall-winter SeaWiFS chl-a peaks in the same area. On the inner shelf, different biogeographic zones were identified close to the major estuaries.

The chl-a pattern changes and their linkages with environmental determinants were explored by using model sensitivity studies and by examining the seasonal to interannual variance of physical forcing. The model sensitivity studies suggested the input of riverine nutrients was not the major influence on chl-a variability on the MAB. This is consistent with the finding that the pathway along which the river water enters the shelf influences how much nitrogen ultimately enters the water on the MAB (Moline et al., 2008). The Hudson River outflow frequently forms a bulge of recirculating fluid that limits the volume of fresh water and is eventually advected away in a coastal current (Chant et al., 2008). During this time, high biological activity can significantly deplete the nutrients in the plume (Moline et al., 2008; Schofield et al., 2013). Friederichs et al. (2019) developed a biogeochemical-circulation model in the study region and concluded that the spatiotemporal variability of the net community production (NCP) is dominated by the along-shelf and cross-shelf nitrogen fluxes onto the MAB. High NCP is found when inorganic nitrogen entering from across the continental slope is high and terrestrial inputs are low. This is consistent with our model sensitivity study, in which the contributions of nutrients from riverine inputs were found to be less significant than other drivers of phytoplankton productivity on the shelf.

Despite the fact that the nutrients associated with plumes play a minor role in stimulating the shelf productivity, the plumes do play a significant role in altering the stability of the water column (Castelao et al., 2008a), which is a primary factor influencing the phytoplankton productivity on the inner shelf of the MAB (Xu et al., 2013). During the winter and pre-spring, low irradiance and deep mixing impose light limitations on

phytoplankton blooms. As the stratification develops with the presence of a buoyant river plume combined with seasonal warming, increased light availability to the phytoplankton promotes growth. Therefore, high Hudson River discharge events in the fall of 2011 combined with the high frequency NW winds resulted in high offshore freshwater transport and stratification in the water column, which was favorable for the phytoplankton growth and high chl-a concentrations found on the New Jersey shelf in the fall of 2011 (Figures 4a, b).

There were significant interannual variabilities in the peak chl-a concentrations, especially in the inner shelf region identified by MODISA EOF mode 2 (Figure 3b, h). A number of factors could be responsible for these anomalies, including record breaking precipitation and river discharge associated with Hurricane Irene and Tropical Storm Lee in 2011 (Munroe et al., 2013), anomalous wind forcing by the upper level jet stream in the winter and spring of 2012 (Chen et al., 2014), or intermittent impacts of large-scale circulation features like Gulf Stream eddies or meanders impinging onto the shelf (Brown et al., 1985, Ryan et al., 1999; Zhang et al., 2015). As suggested in Friederichs et al. (2019), the interannual variability of the net advective flux to the MAB is larger than that from the estuaries and rivers, both in terms of DIN inputs and water volume flux. Other broad-scale circulation patterns at the open boundary of the MAB are significant drivers of ecosystem variability. Better understanding of these local and intermittent atmospheric and oceanic processes will be necessary to further understand the biological phenomena accompanying the large interannual variability in the outer waters directly influenced by offshore forcing.

The ways in which different forcing mechanisms contribute to the PEA and chl-a variability were quantitatively compared in this study. The results obtained from the model experiments demonstrated the capability of sensitivity runs to identify the main contributors to water column stability and its effects on phytoplankton blooms at particular times. However, in these sensitivity experiments, only one forcing factor and one period (fall-spring of 2005-2006) were considered. Over interannual time scales, the combinations of different forcing mechanisms varied. Therefore, for years during which the forcing factors or combinations of forcing factors vary, coupled model sensitivity runs should be applied before interpretation of the results.

4.2 Climate Cycles and Dynamics in the MAB

The shelf waters along the Northeast United States have been undergoing warming (Mountain, 2003) at three times the global average (Saba et al., 2016). On the MAB, the depth-averaged shelf temperature increased by 0.026 °C y^{-1} from 1997 to 2013, which was a significant acceleration of the 37-year positive trend (Forsyth et al., 2015). The changes in temperature distributions might reflect a range of processes affecting the food web. The changes in the patterns of phytoplankton growth reflect the interplay between

bottom-up forces, which directly regulate growth rates, and top-down forces related to phytoplankton loss (e.g., grazing, sinking, lysis) processes. Bottom-up effects can include changes in the phytoplankton productivity and/or composition at the base of the food web (Ji et al., 2010; Hunter-Cevera et al., 2016) or changes in the timing of the blooms. Finally, many of the higher trophic species show physiological thermal thresholds ranges that might drive a redistribution of the higher trophic levels (Friedland et al., 2013; Wahle et al., 2015; Rheuban et al., 2017). The observed chl-a spatial and temporal variability on the MAB was most likely due to forcing changes driven by a number of interacting climate cycles whose effects were superimposed on overall global anthropogenic changes.

The AMO (Kerr, 2000) operates over decadal time scales. The AMO began to transition from a negative to a positive phase in the early-1990s and fully entered a positive-warm phase in 1995 (Enfield et al., 2001). Thus, for the span of this time series, we used satellite data obtained during the warm phase of the AMO, which has been associated with changes in the Atlantic overturning circulation and movement of the Gulf Stream to the north (Zhang et al., 2008). These changes have resulted in an enhanced flow of Gulf Stream slope water into the Gulf of Maine (Saba et al., 2016). Additionally, the movement of the Gulf Stream to the north has the potential to reduce the southward transport of the Labrador sub-arctic slope water. Chl-a variability has been hypothesized to reflect shifts in the AMO that resulted in an increase in the low-frequency cross-shelf winter wind stress by 75% over a decade (Schofield et al., 2008). Winter blooms of phytoplankton are sensitive to light availability and the increase in the winds presumably results in greater mixing of the unstratified water column, thus limiting the light required for phytoplankton growth (Xu et al., 2011; 2013). This study confirms both the continued increase in the overall strength of the winter winds as well as an increase in the proportion (number) of high intensity winds (winter storms), which are associated with blooms that are delayed to the spring season.

The most recent NAO annual index suggests that the NAO was in a positive phase in 2011, crossed over into a negative phase in 2012 and 2013, then switched back to a positive phase in 2014. In a positive phase of the NAO, there is a northward current and an increase in westerly winds along the Northeast United States and Canada (Hurrell & Deser, 2009). These shifts are associated with declining temperatures off of Labrador and northern Newfoundland and increased temperatures in the Mid-Atlantic. These trends are seen in both surface and bottom waters (Kavanaugh et al., 2017). The spring blooms on the MAB are associated with the onset of stratification on the outer shelf, which presumably is partially influenced by the warmer temperatures of the Mid-Atlantic U.S. associated with the NAO positive phase (Chen et al., 2016; Kavanaugh et al., 2017). On the southern part of the MAB in the MODISA EOF mode 3 region, we identified a northward shift of the fall-winter chl-a peak from the coast of Cape Hatteras to the

Virginia coast. Model simulations have shown that in the region of the MAB closest to the Gulf Stream (in the southern part of the MAB), primary production varies significantly (Friederichs et al., 2019). The northward moving chl-a peak could be associated with the Gulf Stream north wall (GSNW), which would allow for the intrusion of deep high-nutrient water onto the shelf and induce phytoplankton blooms (Zhang et al., 2018). Taylor & Stephens (1998) showed that the GSNW is significantly correlated with the northward movement of water during a positive phase of the NAO. Therefore, when interpreting the interannual variabilities of chl-a in the southern part of the MAB near Cape Hatteras, the influence of the climate signal on the Gulf Stream should be considered.

5 Conclusions

EOF analysis of satellite imaging data of surface chl-a on the MAB during the MODISA and SeaWiFS periods identified three major biogeographic zones. It was determined that during both periods, the highest spatial variability occurred on the outer shelf, however, during the MODISA period, the chl-a peak occurred in the spring, whereas it occurred in fall-winter during the SeaWiFS period. The New Jersey shelf was the second dominant biogeographic zone in MODISA period, in which a fall-winter chl-a peak was observed, whereas during the SeaWiFS period, this fall-winter chl-a peak was located in the Delaware Bay estuary. The third biogeographic zone was in the southern part of the MAB near the Virginia coast in the EOF mode 3 region. During the SeaWiFS period, however, the chl-a peak occurred further south near Cape Hatteras in the SeaWiFS EOF mode 3 region.

Climate-sensitive local environmental variables (net heat flux, wind, river discharge) emerged as the most significant factors regulating water column stability, which is important for the timing and magnitude of a phytoplankton bloom. Increased wind mixing along with increased heat loss resulted in a delayed spring bloom on the outer shelf during the MODISA period. The increase in the amount of chl-a on the New Jersey shelf in the fall during the MODISA period was associated with high river discharge events. The anomalously high chl-a in the coastal waters of Cape Hatteras was correlated with high Chesapeake Bay rivers' discharge in fall and winter, and a northward expansion of the high chl-a zone during the MODISA period was detected. The results of our study improve our understanding of the regional linkages between phytoplankton dynamics and multiple climate-sensitive environmental drivers.

Acknowledgments

This work was supported by the National Science Foundation of China (grant number 41606025); the National Key R&D Program of China (grant number 2016YFA0600903), and the Mid-Atlantic Regional Association Coastal Ocean Observing System (MARACOOS) (grant number NA16NOS0120020) funded by NOAA's Integrated

740 Ocean Observing System. We thank the scientists at the Rutgers University's Center of
741 Ocean Observing Leadership (RU COOL) for their support. We are grateful for the
742 constructive comments and suggestions by the anonymous reviewers.

743 **References**

744 Bi, H. S., Peterson, W. T., Lamb, J., & Casillas, E. (2011). Copepods and salmon:
745 Characterizing the spatial distribution of juvenile salmon along the Washington and
746 Oregon coast, USA. *Fisheries Oceanography* 20, 125-138.

747 Biscaye, P.E., Flagg, C.N., & Falkowski, P. (1994). The Shelf Edge Exchange Processes
748 experiment, SEEP-II: an introduction to hypotheses, results and conclusions. *Deep-Sea*
749 *Res. II* 41, 231–252.

750 Bowers, D.G., Braithwaite, K.M., Nimmo-Smith, W.A.M., Graham, G.W. (2011). The
751 optical efficient of flocs in shelf seas and estuaries. *Estuarine, Coastal and Shelf*
752 *Science*, 91 (2011), pp. 341-350.

753 Brown, O.B., Evans, R. H., Brown, J. W., Gordon, H. R., Smith, R. C., & Baker, K. S.
754 (1985). Phytoplankton blooming off the U.S. east coast: A satellite description, *Science*,
755 229(4709), 163–167.

756 Castelao, R., Schofield, O., Glenn, S., Chant, R., & Kohut, J. (2008a). Cross-shelf
757 transport of freshwater on the New Jersey shelf. *Journal of Geophysical Research*, 113,
758 C07017. https://doi.org/10.1029/2007JC004241.

759 Castelao, R., Glenn, S., Schofield, O., Chant, R., Wilkin, J., & Kohut, J. (2008b).
760 Seasonal evolution of hydrographic fields in the central Middle Atlantic Bight from
761 glider observations. *Geophysical Research Letters*. 35, L03617.
762 https://doi.org/10.1029/2007GL032335.

763 Castelao, R., Glenn, S., & Schofield, O. (2010). Temperature, salinity, and density
764 variability in the central Middle Atlantic Bight. *Journal of Geophysical Research*, 115,
765 C10005. http://dx.doi.org/10.1029/2009JC006082.

766 Chant, R.J., Glenn, S.M., Hunter, E., Kohut, J., Chen, R.F., Houghton, R.W., Bosch, J., &
767 Schofield, O. (2008). Bulge Formation of a Buoyant River Outflow. *Journal of*
768 *Geophysical Research*, 113, C01017. https://doi.org/10.1029/2007JC004100.

769 Chen, K., Gawarkiewicz, G.G., Lentz, S.J., & Bane, J.M. (2014). Diagnosing the
770 warming of the Northeastern US Coastal Ocean in 2012: A linkage between the
771 atmospheric jet stream variability and ocean response. *Journal of Geophysical*
772 *Research: Oceans*, 119, 218–227. https://doi.org/10.1002/2013JC009393.

773 Chen, K., Kwon, Y.-O., & Gawarkiewicz, G. (2016). Interannual variability of
774 winter-spring temperature in the Middle Atlantic Bight: Relative contributions of
775 atmospheric and oceanic processes. *Journal of Geophysical Research: Oceans*, 121,
776 4209–4227. https://doi.org/10.1002/2016JC011646.

777 Curry, R.G., & McCartney, M.S. (2001). Ocean gyre circulation changes associated with
778 the North Atlantic Oscillation. *Journal of Physical Oceanography*, 31, 3374–3400.

779 Dickson, R.R., Lazier, J., Meinke, J., Rhines, P., & Swift, J. (1996). Long-term
780 coordinated changes in the convective activity of the North Atlantic. *Progress in*
781 *Oceanography*, 38, Pergamon Press, 241–295.

782 Enfield, D. B., & Mestas-Nunez, A. M. (1999). Multiscale variabilities in global SST and
783 their relationships with tropospheric climate patterns. *Journal of Climate*, 12, 2719–
784 2733.

785 Enfield, D.B., Mestas-Nunez, A.M., & Trimble, P.J. (2001). The Atlantic Multidecadal
786 Oscillation and its relationship to rainfall and river flows in the continental U.S..
787 *Geophysical Research Letters*, 28, 2077-2080.

788 Fairall, C.W., Bradley, E.F., Hare, J.E., Grachev, A.A., & Edson, J.B. (2003). Bulk
789 parameterization of air-sea fluxes: updates and verification for the COARE algorithm.
790 *Journal of Climate*, 19 (4), 571–591.

791 Fasham, M.J.R., Ducklow, H.W., & McKelvie, S.M. (1990). A nitrogen- based model of
792 plankton dynamics in the oceanic mixed layer. *Journal of Marine Research*, 48, 591–
793 639.

794 Fennel, K., Wilkin, J., Levin, J., Moisan, J., O'Reilly, J., & Haidvogel, D. (2006).
795 Nitrogen cycling in the Middle Atlantic Bight: Results from a three-dimensional model
796 and implications for the North Atlantic nitrogen budget. *Global Biogeochemical Cycles*,
797 20, GB3007. https://doi.org/10.1029/2005GB002456.

798 Friedland, K.D., Kane, J., Hare, J.A., Lough, R.G., Fratantoni, P.S., Fogarty, M.J., &
799 Nye, J.A. (2013). Thermal habitat constraints on zooplankton species associated with
800 Atlantic cod (Gadus morhua) on the US Northeast Continental Shelf. *Progress in*
801 *Oceanography*, 116, 1–13.

802 Friedrichs, M. A. M., St-Laurent, P., Xiao, Y., Hofmann, E., Hyde, K., Mannino, A., et
803 al. (2019). Ocean circulation causes strong variability in the Mid-Atlantic Bight
804 nitrogen budget. *Journal of Geophysical Research: Oceans*, 124, 113–134.
805 https://doi.org/10.1029/2018JC014424

Forsyth, J.S.T., Andres, M., & Gawarkiewicz, G.G. (2015). Recent accelerated warming of the Continental Shelf off New Jersey: Observations from the CMV Oleander expendable bathythermograph line. *Journal of Geophysical Research: Oceans*, 120, 2370–2384. https://doi.org/ 10.1002/2014JC010516.

Fulweiler, R.W., Oczkowski, A.J., Miller, K.M., Oviatt, C.A., & Pilson, M.E.Q. (2015). Whole truths vs. half truths–and a search for clarity in long-term water temperature records. *Estuarine, Coastal and Shelf Science*, 157, A1–A6.

Gregg, W.W., & Casey, N.W. (2010). Improving the consistency of ocean color data: A step toward climate data records. *Geophysical Research Letters*, 37, L04605. https://doi.org/10.1029/2009gl041893.

Gong, D., Kohut, J.T., & Glenn, S.M. (2010), Seasonal climatology of wind-driven circulation on the New Jersey Shelf. *Journal of Geophysical Research*. vol 115, C04006, https://doi.org/10.1029/2009JC005520.

Haidvogel, D.B., Beckman A., (1999). *Numerical Ocean Circulation Modeling*. Imperial College Press, 318 pp.

Hammond, M.L., Beaulieu, C., Henson, S.A., & Sahu, S.K. (2018). Assessing the presence of discontinuities in the ocean color satellite record and their effects on chlorophyll trends and their uncertainties. *Geophysical Research Letters*, 45. https://doi.org/10.1029/2017GL076928.

Hofmann, E.E., Cahill, B., Fennel, K., Friedrichs, M.A.M., Hyde, K., Lee, C., Mannino, A., Najjar, R.G., O'Reilly, J.E., Wilkin, J., & Xue, J. (2011). Modeling the dynamics of continental shelf carbon. *Annual Review of Marine Science*, 3, 93–122.

Houghton, R., Schlitz, R., Beardsley, R., Butman, B., & Chamberlin, J. (1982). The Middle Atlantic Bight cold pool: evolution of the temperature structure during Summer 1979. *Journal of Geophysical Research*, 12, 1019–1029.

Howarth R.W. et al. (1996). Regional nitrogen budgets and riverine N & P fluxes for the drainages to the North Atlantic Ocean: Natural and human influences. In: Howarth R.W. (eds). *Nitrogen Cycling in the North Atlantic Ocean and its Watersheds*. Springer, Dordrecht.

Hu, C., Lee, Z., & Franz, B.A. (2012). Chlorophyll-a algorithms for oligotrophic oceans: A novel approach based on three-band reflectance difference, *Journal of Geophysical Research*, 117, C01011. https://doi.org/10.1029/2011JC007395.

838 Hunter-Cevera, K.R., Neubert, M.G., Olson, R.J., Solow, A.R., Shalapyonok, A., &
839 Sosik, H.M. (2016). Physiological and ecological drivers of early spring blooms of a
840 coastal phytoplankter. *Science*, 354(6310), 326–329.

841 Hurrell, J.W. (1995). Decadal trends in the North-Atlantic Oscillation: Regional
842 temperatures and precipitation. *Science*, 269(5224), 676–679,
843 doi:10.1126/science.269.5224.676.

844 Hurrell, J.W., & Deser, C. (2009). North Atlantic climate variability: the role of the north
845 atlantic oscillation. *Journal of Marine System*, 78, 28–41.

846 Ji, R., Edwards, M., Mackas, D.L., Runge, J.A., & Thomas, A.C. (2010). Marine
847 plankton phenology and life history in a changing climate: Current research and future
848 directions. *Journal of Plankton Research*, 32, 1355–1368.

849 Jiang, L. & Xia, M, (2018). Modeling investigation of the nutrient and phytoplankton
850 variability in the Chesapeake Bay outflow plume, *Progress in Oceanography*, 162,
851 290-302.

852 Kavanaugh, M.T., Rheuban, J.E., Luis, K.M.A., & Doney, S.C. (2017). Thirty-three years
853 of ocean benthic warming along the U.S. Northeast Continental Shelf and Slope:
854 Patterns, drivers, and ecological consequences. *Journal of Geophysical Research:*
855 *Oceans*, 122. https://doi.org/10.1002/ 2017JC012953.

856 Kerr, R.A. (2000). A North Atlantic climate pacemaker for the centuries. *Science*, 288
857 (5473), 1984–1986.

858 Lentz, S., Shearman, K., Anderson, S., Plueddemann, A., & Edson, J. (2003). Evolution
859 of stratification over the New England shelf during the Coastal Mixing and Optics
860 study, August 1996–June 1997. *Journal of Geophysical Research*, 108(C1), 3008.
861 https://doi.org/10.1029/2001JC001121.

862 Marshall, J., Johnson, H., & Goodman, J. (2001). A study of the interaction of the North
863 Atlantic Oscillation with ocean circulation. *Journal of Climate*, 14, 1399–1421.

864 Mesinger, F., DiMego, G., Kalnay, E., Mitchell, K., Shafran, P. C., Ebisuzaki, W., … &
865 Shi, W. (2006). North American Regional Reanalysis. *Bulletin of the American*
866 *Meteorological Society*, 87, 343–360.

867 Moline, M.A., Frazer, T.K., Chant, R., Glenn, S., Jacoby, C.A., Reinfelder, J.R., Yost, J.,
868 Zhou, M., & Schofield, O. (2008). Biological responses in a dynamic, buoyant river
869 plume. *Oceanography*, 21, 71 – 89.

Mountain, D.G. (2003). Variability in the properties of Shelf Water in the Middle Atlantic Bight, 1977–1999. *Journal of Geophysical Research*, 108(C1), 3014. https://doi.org/10.1029/2001JC001044.

Munroe, D., Tabatabai, A., Burt, I., Bushek, D., Powell, E. N., & Wilkin, J. (2013). Oyster mortality in Delaware Bay: Impacts and recovery from Hurricane Irene and Tropical Storm Lee. *Estuarine, Coastal and Shelf Science,* 135, 209–219. https://doi.org/10.1016/j.ecss.2013.10.011.

National Marine Fisheries Service. 2015. Fisheries of the United States 2015. Report FUS2015.

O'Reilly, J., & Busch, D.A. (1984). Phytoplankton primary production on the northwestern Atlantic Shelf. Rapports et Proces-Verbaux des Reunions Conseil International pour l'Exploration de la Mer. 183, 255–268.

Oschlies, A. (2001). NAO induced long-term changes in nutrient supply to the surface waters of the North Atlantic, *Geophysical Research Letters*, 28(9), 1751–1754, doi:10.1029/2000GL012328.

Pinsky, M.L., Worm, B., Fogarty, M.J., Sarmiento, J.L., & Levin, S.A. (2013). Marine taxa track local climate velocities. *Science*, 341(6151), 1239–1242.

Platt, T., White, III G.N., Zhai, L., Sathyendranath, S., Roy, S. (2009). The phenology of phytoplankton blooms: ecosystem indicators from remote sensing. *Ecological Modelling*, 220, 3057–3069.

Powell, E.N., & Mann R. (2005). Evidence of recent recruitment in the ocean quahog Arctica islandica in the Mid-Atlantic Bight. *Journal of Shellfish Research*, 24(2), 517-530.

Rheuban, J.E., Kavanaugh, M.T., & Doney, S.C. (2017). Implications of future northwest Atlantic bottom temperatures on the American Lobster (Homarus americanus) fishery. *Journal of Geophysical Research: Oceans*, 122. https://doi.org/10.1002/2017JC012949.

Ryan, J.P., Yoder, J.A., & Cornillon, P.C. (1999). Enhanced Chl-a at the Shelfbreak of the Mid-Atlantic Bight and Georges Bank during the Spring Transition. *Limnology and Oceanography*, 44, 1–11.

Ryther, J.H., & Dunstan, W.M. (1971). Nitrogen, phosphorus, and eutrophication in the coastal marine environment. *Science*, 171, 1008–1112.

902 Saba, V. S., et al. (2016). Enhanced warming of the Northwest Atlantic Ocean under
903 climate change, *Journal of Geophysical Research: Oceans*, 121, 118–132.
904 https://doi.org/10.1002/2015JC011346.

905 Schofield, O., Chant, R., Cahill, B., Castelao, R., Gong, D., Kohut, J., Montes-Hugo, M.,
906 Ramanduri, R., Xu, Y., & Glenn, S. (2008). The decadal view of the Mid-Atlantic Bight
907 from the COOLroom: Is our coastal system changing? *Oceanography*, 23(4), 108–117.

908 Schofield, O., Moline, M.A., Cahill, B., Frazer, T., Kahl, A., Oliver, M., Reinfelder, J.,
909 Glenn, S., & Chant, R. (2013). Phytoplankton productivity in a turbid buoyant coastal
910 plume. *Continental Shelf Research*. https://doi.org/10.1016/j.csr.2013.02.005.

911 Sharp, J.H., & Church, T. M. (1981). Biochemical modeling in coastal waters of the
912 Middle Atlantic States. *Limnology and Oceanography*, 26 (5), 843–854.

913 Shearman, K., & Lentz, S. J. (2004). Observations of tidal variability on the New
914 England shelf, *Journal of Geophysical Research*, 109, C06010,
915 doi:10.1029/2003JC001972.

916 Simpson, J.H., Hughes, D.G., & Morris, N.C.G. (1977). The relation of seasonal
917 stratification to tidal mixing on the continental shelf. A Voyage to Discovery. *Deep-Sea*
918 *Research* (Suppl.), 327–340.

919 Simpson, J.H., & Bowers, D. (1981). Models of stratification and frontal movement in
920 shelf seas. *Deep-Sea Research*, 28A, 727–738.

921 Shearman, R.K., & Lentz, S.J. (2010). Long-term sea surface temperature variability
922 along the U.S. East Coast. *Journal of Physical Oceanography*, 40, 1004–1017.

923 Taylor, A.H., & Stephens, J.A. (1998). The North Atlantic Oscillation and the latitude of
924 the Gulf Stream. *Tellus*, 50A: 134–142.

925 Trenberth, K.D., Shea, D.J. (2005). Atlantic hurricanes and natural variability in
926 2005. *Geophysical Research Letters*, 33, L12704.
927 https://doi.org/10.1029/2006GL026894.

928 Wahle, R.A., Dellinger, L., Olszewski, S., & Jekielek, P. (2015). American lobster
929 nurseries of southern New England receding in the face of climate change. *ICES*
930 *Journal of Marine Science*, 72(Suppl 1), i69–i78.

931 Wilkin, J.L., Arango, H.G., Haidvogel, D.B., Lichtenwalner, C.S., Glenn, S.M., &
932 Hedström, K.S. (2005). A regional ocean modeling system for the Long-term

933 Ecosystem Observatory. *Journal of Geophysical Research*, 110, C06S91.
934 https://doi.org/10.1029/2003JC002218.

935 Wilkin, J.L. (2006). The summertime heat budget and circulation of southeast new
936 England shelf waters, *Journal of Physical Oceanography*, 36(11), 1997–2011.
937 https://doi.org/10.1175/JPO2968.1.

938 Wilkin, J.L.& Hunter, E.J. (2013). An assessment of the skill of real-time models of
939 Mid-Atlantic Bight continental shelf circulation. *Journal of Geophysical Research*, 118,
940 2919–2933. https://doi.org/10.1002/jgrc.20223.
941
942 Wirick, C.D. (1994). Exchange of phytoplankton across the continental shelf-slope
943 boundary of the Middle Atlantic Bight during spring 1988. *Deep Sea Research Part II*:
944 41, 391-410.

945 Xu, Y., Chant, R., Gong, D., Castelao, R., Glenn, S., & Schofield, O. (2011). Seasonal
946 variability of chl-a a in the Mid-Atlantic Bight. *Continental Shelf Research*, 31(16),
947 1640-1650. https://doi.org/10.1016/j.csr.2011.05.019.

948 Xu, Y., Cahill, B., Wilkin, J., & Schofield O. (2013). Role of wind in regulating
949 phytoplankton blooms on the Mid-Atlantic Bight. *Continental Shelf Research*, 63(4),
950 S26-S35. https://doi.org/10.1016/j.csr.2012.09.011.

951 Yoder, J.A., O'Reilly, J.E., Barnard, A.H., Moore, T.S., & Ruhsam, C.M. (2001).
952 Variability in coastal zone color scanner (CZCS) Chl-a imagery of ocean margin waters
953 off the US East Coast. *Continental Shelf Research*, 21(11-12), 1191 – 1218.

954 Yoder, J.A., Schollaert, S.E., & O'Reilly, J.E. (2002). Climatological Phytoplankton
955 Chl-a and Sea Surface Temperature Patterns in Continental Shelf and Slope Waters off
956 the Northeast U.S. Coast. *Limnology and Oceanography*, 3, 672 – 682.

957 Zhang, R. (2008). Coherent surface-subsurface fingerprint of the Atlantic meridional
958 overturning circulation, *Geophysical Research Letters*, 35, L20705.
959 https://doi.org/10.1029/2008GL035463.

960 Zhang, S., Curchitser, E. N., Kang, D., Stock, C. A., & Dussin, R. (2018). Impacts of
961 mesoscale eddies on the vertical nitrate flux in the Gulf Stream region. *Journal of*
962 *Geophysical Research: Oceans*, 123, 497–513. https://doi.org/10.1002/2017JC013402.

963 Zhang, W.G., & Gawarkiewicz, G.G. (2015). Dynamics of the direct intrusion of Gulf
964 Stream ring water onto the Mid-Atlantic Bight shelf. *Geophysical Research Letters*, 42,
965 7687–7695. https://doi.org/10.1002/2015GL065530.